Journal of the Optical Society of America A
OPTICS, IMAGE SCIENCE, AND VISION

Light propagation analysis using a translated plane angular spectrum method with the oblique plane wave incidence

HYEON-HO SON[1,2] AND KYUNGHWAN OH[2,*]

[1]R&D Center, LG Display, Paju-si, Gyeonggi-do 413-811, South Korea
[2]Department of Physics, Yonsei University, Seodaemun-gu, Seoul 120-749, South Korea
*Corresponding author: koh@yonsei.ac.kr

Received 11 December 2014; revised 25 March 2015; accepted 25 March 2015; posted 25 March 2015 (Doc. ID 230601); published 29 April 2015

A novel angular spectrum method was proposed to numerically analyze off-axis free-space light propagation on a translated plane to an arbitrary angle. Utilizing a shifted angular spectrum method based on an oblique incident plane wave assumption, a generalized light propagation formulation was obtained in a wide range of both tilt angles and sampling intervals, which overcame the limitations of prior attempts. A detailed comparison of the proposed angular spectrum method with prior methods is numerically presented for diffractive optics and computer-generated holograms. The validity of the proposed method was confirmed experimentally by reconstructing a digital holographic image using a spatial light modulator.

OCIS codes: (050.1940) Diffraction; (090.1760) Computer holography; (070.0070) Fourier optics and signal processing.

http://dx.doi.org/10.1364/JOSAA.32.000949

1. INTRODUCTION

Light propagation between two parallel planes has been analyzed in depth by various numerical methods based on a scalar diffraction theory [1,2]. The Fresnel transform method and Huygens integral method have been major tools for numerically analyzing light diffraction and propagation [1]. These methods have played important roles in signal processing for digital holography (DH) [3,4] and computer-generated holograms (CGHs), as well as three-dimensional displays [5,6]. However, prior analyses have shown critical limitations in dealing with current optical issues because of their common fundamental assumptions: (1) the diffracted light propagation axis is nearly parallel to the input optic axis, and (2) the object plane and image plane are parallel to each other. However, in current wide angle displays, as schematically shown in Fig. 1(a), there is an increasing demand to analyze the light propagation between nonparallel planes or off-axis propagation with a significantly large angle, which could not be analyzed in the prior techniques [6].

The angular spectrum method (ASM), which was rigorously derived from the Rayleigh–Sommerfeld integral, has been attempted as an alternative to the prior methods, especially in analyzing the diffraction between tilted planes [7–9]. However, all of the rotated wave vector components should be identified to use the ASM. This requires a nontrivial transform based on a nonuniform sampling interval in the Fourier plane, which has created serious computational complexities [10,11].

As one of the on-axis ASMs, the band-limited angular spectrum method (BL-ASM) further expanded the calculation area, along with zero padding using a similar formulation as the conventional on-axis ASM [12]. However, BL-ASM was still limited by the tilt angle and extensive computational requirements. Recently, shifted plane propagation methods have been introduced as another category of numerical light propagation analysis [12–14]. The shifted Fresnel method (Shift-FR) was reported first to cope with a wider tilt angle, but it suffered from aliasing in a short distance between the object-image planes [13]. This weakness was improved by the shifted angular spectrum method (Shift-ASM), which showed a good convergence to BL-ASM analyses.

However, the Shift-ASM still required a narrow range of the tilted angle and a long distance between the planes, which are fundamentally the same limitations as the BL-ASM [14].

In this paper, a new and general numerical method is proposed for analyzing the off-axis light propagation on a translated plane to an arbitrary angle. By assuming an oblique plane wave incidence, a general formula was established and named Translated-Plane ASM or Translated-ASM. Translated-ASM can provide valid numerical results for arbitrary incidence angle and sampling interval, overcoming the fundamental limitations of prior methods. We compared our Translated-ASM with prior methods to confirm its validity in numerical simulations.

We also experimentally confirmed the validity of the Translated-ASM by reconstructing holographic images on a

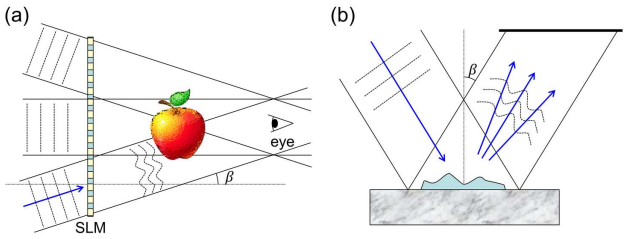

Fig. 1. Applications of the translated-plane calculation method on (a) three-dimensional holographic display using off-axis holography and (b) retrieval of off-axis phase information in digital holographic microscopy (SLM, spatial light modulator; β, tilt angle).

plane along a tilted axis using a phase-only spatial light modulator (SLM), and comparing them with Translated-ASM numerical results. The proposed numerical method can be applied directly to reconstructing a hologram on the tilted axis or analyzing the off-axis phase information of an object in the digital holographic microscopy, as illustrated in Fig. 1(b). Our Translated-ASM formalism can provide a new potential in next-generation wide-angle holography, as well as advanced holographic microscopy.

2. FORMULATION OF THE TRANSLATED PLANE ANGULAR SPECTRUM METHOD

The coordinate system used in this study is shown in Fig. 2. The image plane coordinates, (x', y', z'), are shifted horizontally along the x axis in reference to the object plane coordinates, (x, y, z), by Eq. (1):

$$x' = x + Z \tan\beta$$
$$z' = Z. \quad (1)$$

In the conventional ASM, the output electric field, E_o, is given in terms of the input electric field, E_i, multiplied by the propagation phase factor, $\exp(ik_zZ)$, as in Eq. (2) [1,2]:

$$E_o(x', y'; Z) = \mathcal{F}^{-1}\{\mathcal{F}[E_i(x, y; 0)]\exp(ik_zZ)\}[k_x, k_y]. \quad (2)$$

Here, $\mathcal{F}(\cdot)$ and $\mathcal{F}^{-1}(\cdot)$ denote the three-dimensional Fourier and inverse Fourier transform operator, and $[k_x, k_y]$ represents the spatial frequency variables. Using the shifted coordinates in Eq. (1), we can obtain an integral equation:

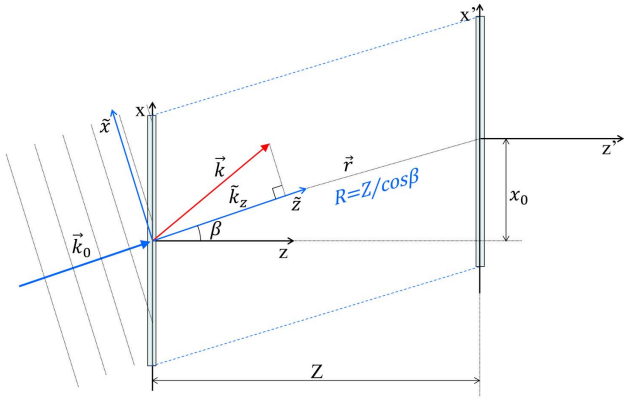

Fig. 2. Coordinate systems for a horizontally shifted plane. Z is the propagation distance between two planes, and β is the tilted angle.

$$E_o(x', y'; Z) = \iint A_i(k_x, k_y)e^{iR(k_z\cos\beta - k_x\sin\beta)}e^{i(k_xx' + k_yy')}\mathrm{d}k_x\mathrm{d}k_y. \quad (3)$$

Here, the distance between two planes is replaced by the effective distance along the tilted direction ($R = Z/\cos\beta$). Using the rotational transform of the wave vectors in the input field as shown in Eq. (4), the first phase term in Eq. (3) can be further replaced by $\tilde{k}_z$, a component of the wave vector rotated by the tilted angle β. This rotated wave vector component can be interpreted as a projected wave vector of an angular spectrum onto the tilted axis:

$$\begin{pmatrix}\tilde{k}_x \\ \tilde{k}_z\end{pmatrix} = \begin{pmatrix}\cos\beta & \sin\beta \\ -\sin\beta & \cos\beta\end{pmatrix}\begin{pmatrix}k_x \\ k_z\end{pmatrix}$$
$$\rightarrow \tilde{k}_z = k_z\cos\beta - k_x\sin\beta = \vec{\mathbf{k}}\cdot\hat{\mathbf{r}}. \quad (4)$$

Then, we obtain the Shifted-ASM using the convolution theorem:

$$E_o(x', y') = \mathcal{F}^{-1}(\mathcal{F}(E_i(x, y; 0))\exp(i\tilde{k}_zR))[k_x, k_y]. \quad (5)$$

Note that the above expression is identical to that of the prior Shifted-ASM [14], if we replace $-Z\tan\beta$ with the lateral shift distance, x_0. Here, the phase variation, $\tilde{k}_zR$, corresponds to the projection of an angular spectrum component onto the tilted axis.

We further assumed that the incident light is a plane wave illuminated along the tilted axis such that the input electric field is expressed as in the following equation:

$$E_i(x, y; 0) = m(x, y)E_r(x, y; 0) = m(x, y)A_re^{-ik_0x\sin\beta}. \quad (6)$$

Here, $m(x, y)$ is the modulation function of the input electric field on the object plane. By changing the integration variables to the shifted wave vector components,

$$\kappa_x \equiv k_x + k_0\sin\beta = k_x + k_{0x}, \qquad \kappa_y \equiv k_y, \quad (7)$$

we obtained

$$E_o(x', y') = A_re^{-ik_0x'\sin\beta} \times \iint\left[\iint m(x, y)e^{-i(\kappa_xx + \kappa_yy)}\mathrm{d}x\mathrm{d}y\right]e^{i\tilde{k}_zR}e^{i(\kappa_xx' + \kappa_yy')}\mathrm{d}\kappa_x\mathrm{d}\kappa_y. \quad (8)$$

Here, we have $\tilde{k}_z = \cos\beta\cdot[k_0^2 - (\kappa_x - k_0\sin\beta)^2 - \kappa_y^2]^{1/2} - (\kappa_x - k_0\sin\beta)\sin\beta$ by using the coordinate rotation in Eq. (4) and the wave vector relation, $k_x^2 + k_y^2 + k_z^2 = k_0^2$. Note that the first factor in Eq. (8), $A_r\exp(-ik_0x'\sin\beta)$, can be taken out of the integral and is interpreted as the reference field propagating toward the shifted plane. The rest of the integrals correspond to the lateral contribution. Using the Fourier integral, Eq. (8) is further reduced to Eq. (9), which serves as our new formalism, "Translated-ASM":

$$E_o(x', y') = E_r(x', y')\cdot\mathcal{F}^{-1}\{\mathcal{F}[m(x, y)]\exp(i\tilde{k}_zR)\}[\kappa_x, \kappa_y]. \quad (9)$$

Note that the input field distribution, $E_i(x, y; 0)$, of the Shift-ASM in Eq. (5) includes a highly oscillating term for a large incident angle, which requires a higher density sampling

grid of the input plane arranged in a nonlinear manner. In contrast, the proposed formalism (Translated-ASM) takes the input field out of the Fourier integral as in Eq. (9). This separation of the reference field from the lateral modulation can allow the efficient simulation of the light propagation along the tilted axis at an arbitrary angle with an arbitrary sampling interval, which was not possible in prior methods.

This method can be further generalized in an arbitrary tilted axis. As shown in Fig. 3, the sampling window is shifted by a lateral displacement, (x_0, y_0). Here, we defined a displacement vector, $\vec{r}$, which is the directional vector from the input plane toward the output plane, and a wave vector, $\vec{k}_0$, of the incident reference beam is also defined in Eq. (10):

$$\vec{\mathbf{r}} \equiv x_0\hat{\mathbf{x}} + y_0\hat{\mathbf{y}} + Z\hat{\mathbf{z}}, \qquad R = |\vec{\mathbf{r}}|$$
$$\vec{\mathbf{k}}_\mathbf{0} = k_0\frac{\vec{\mathbf{r}}}{R} \equiv k_{0x}\hat{\mathbf{x}} + k_{0y}\hat{\mathbf{y}} + k_{0z}\hat{\mathbf{z}}. \tag{10}$$

The shifted wave vector is defined below:

$$\vec{\kappa} \equiv \vec{\mathbf{k}} + \vec{\mathbf{k}}_\mathbf{0}. \tag{11}$$

The phase term in Eq. (10) can be expressed as

$$\tilde{k}_z R = \vec{\mathbf{k}} \cdot \vec{\mathbf{r}} = (\vec{\kappa} - \vec{\mathbf{k}}_\mathbf{0}) \cdot \vec{\mathbf{r}}. \tag{12}$$

Substituting the above equations into Eq. (9), we obtain the generalized formulation for Translated-ASM:

$$E_o(x', y') = E_r(x', y') \times \mathcal{F}^{-1}\{\mathcal{F}[m(x, y)]\exp[i(\vec{\kappa} - \vec{\mathbf{k}}_\mathbf{0}) \cdot \vec{\mathbf{r}}]\}[\kappa_x, \kappa_y]. \tag{13}$$

Here, we have the relation between the wave vectors, $\kappa_z = [k_0^2 - (\kappa_x - k_{0x})^2 - (\kappa_y - k_{0y})^2]^{1/2} + k_{0z}$, using the definition in Eq. (11) and the wave vector relation, $k_x^2 + k_y^2 + k_z^2 = k_0^2$. The first term in Eq. (13) corresponds to the incident electric field and the remaining term to the diffraction of the lateral modulation of the incident light. Note that the momentum change, $\vec{\kappa} - \vec{k}_0$ in Eq. (13) is analogous to the scattered wave vector in the scattering theory [15]. Physically, the light propagation between nonparallel planes or the off-axis propagation with a significantly large angle can be treated as a scattering problem from a two-dimensional laminar scattering source, with the propagation distance sufficiently larger than the object dimension. In the special case of normal plane wave incidence, $(x_0 = y_0 = k_{0x} = k_{0y} = 0)$, we have an equation equivalent to the conventional ASM, as in Eq. (2).

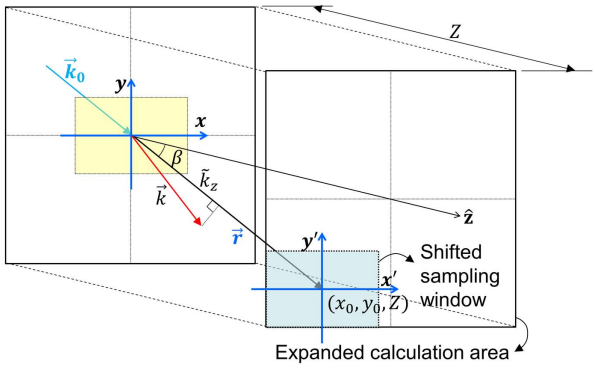

Fig. 3. Generalized coordinates for the propagation along a tilted axis.

3. NUMERICAL SIMULATION USING THE TRANSLATED PLANE ANGULAR SPECTRUM METHOD

As in Fig. 2, a reference plane wave is assumed to be incident on the input screen making a tilt angle of β with respect to the x-direction. A monochromatic wave with the wavelength of $\lambda = 633$ nm is used in this simulation. The diffraction field on the output plane at the propagation distance Z was calculated based on Eq. (13) using MATLAB (R2010A 64 bit version). Here, the modulation function at the input screen was assumed to have the sampling interval of $\Delta x = 1$ μm, $\Delta y = 1$ μm, and the sampling points of $N_x = 1024$ and $N_y = 768$.

At first, we compared the diffraction images of the proposed Translated-ASM with those of the BL-ASM. By using the BL-ASM, the diffracted fields can be extracted in the shifted sampling window, as illustrated in a shaded box in Fig. 3. In the simulations, we started with a small tilt angle of $\beta = 1.0°$ and a circular aperture with a diameter of 300 μm, and the propagation distance were varied from 1000 to 2000 μm.

The intensity and phase images calculated by the BL-ASM are shown in Figs. 4(a) and 4(b). The boxes in Figs. 4(a) and 4(b) are the extracted sampling window, which were used commonly in the Shifted-ASM and Translated-ASM. The images calculated by the Translated-ASM, presented in Figs. 4(c) and 4(d), showed almost the same patterns as those of the BL-ASM. We further analyzed the root-mean-square (RMS) intensity and the phase difference between the calculated images, defined by the below equation:

$$\eta \equiv \sqrt{\sum_{I_A > I_0}\left[\frac{I_T(x, y) - I_B(x, y)}{I_B(x, y)}\right]^2}. \tag{14}$$

Here, I_B and I_T are the normalized intensity calculated by BL-ASM and Translated-ASM, respectively. We used a relatively low intensity limit, $I_0 = 0.5\%$, to avoid the singularity problem. The RMS intensity differences as a function of the propagation distance, Z, were plotted in Fig. 4(e). The

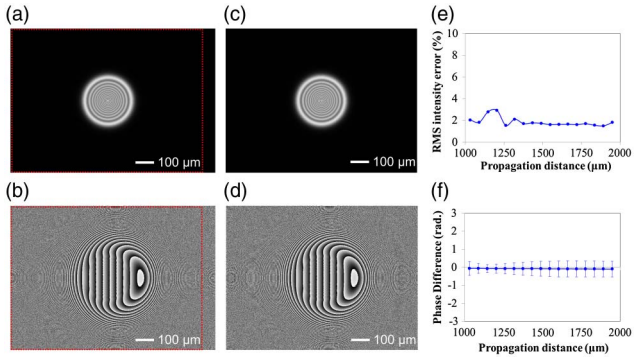

Fig. 4. Calculation diffraction analyses of a circular aperture at the tilt angle $\beta = 1.0°$. (a) Intensity and (b) phase image using BL-ASM at $Z = 1032$ μm; (c) intensity and (d) phase image using the Translated-ASM at $Z = 1032$ μm; and (e) RMS intensity difference and (f) RMS phase difference between Translated-ASM and BL-ASM.

RMS intensity difference showed a small difference less than 3.0% in the entire range of the propagation distance. The phase images also showed a negligible difference between Translated-ASM and BL-ASM, as in Fig. 4(f). These two results confirmed that our Translated-ASM provided numerical analyses consistent to prior BL-ASM for a small tilt angle.

We further investigated the impacts of an extended tilt angle by setting $\beta = 10°$ on three different numerical methods: (i) the conventional on-axis ASM given by Eq. (2), (ii) Shift-ASM given by Eq. (5), and (iii) our Translated-ASM given by Eq. (13). We compared the calculated intensity images at the propagation distances of $Z = 600$ μm, as shown in Fig. 5. The first column corresponds to the conventional on-axis ASM, the second column is the Shift-ASM, and the third is our Translated-ASM. A distinctive nature in these methods could be observed for a large tilt angle. For a narrow sampling interval of $\Delta x = \Delta y = 1$ μm as in Fig. 5(a), we found nearly identical diffraction patterns for the Shift-ASM and Translated-ASM. In contrast, the on-axis ASM resulted in an image shifted to the negative x direction. As we further increase either the sampling interval to $\Delta x = \Delta y = 2$ μm, or the tilt angle to $\beta = 30°$, we observed substantial differences in the three methods as shown in Figs. 5(b) and 5(c), respectively. By increasing the sampling interval, we observed moving images for the Shift-ASM, as well as for BL-ASM in Fig. 5(b), which is consistent to previously reported limitations of these methods producing false images, either at a large sampling interval or a large tilt angle [14]. In the Shift-ASM, the incident field has highly oscillating phase terms in the real space and sparse sampling points cannot properly take account of the rapid oscillatory property [14]. In contrast, our Translated-ASM can effectively separate the phase factor from the Fourier integral as in Eq. (13) to avoid image shifts. For a significantly large tilt angle $\beta = 30°$, only the Translated-ASM showed the correct diffraction patterns maintaining the stationary image positions, as shown in Fig. 5(c). Comparing three numerical methods in Fig. 5, we confirmed that our Translated-ASM can provide more accurate and correct diffraction images than prior methods for either a wider tilt angle or a larger sampling interval.

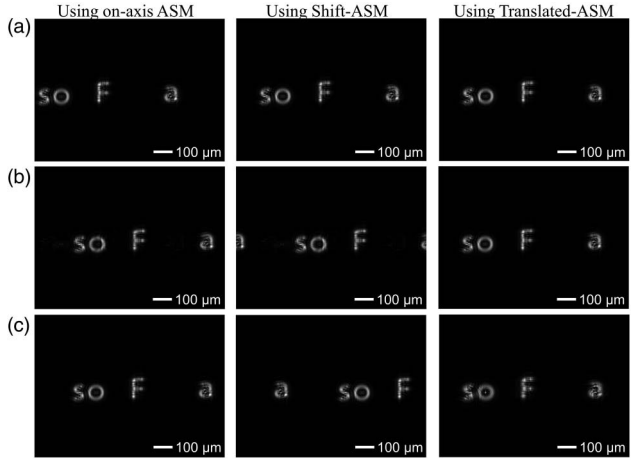

Fig. 5. Diffraction images calculated by three different methods: (a) tilt angle $\beta = 10°$, sampling interval $\Delta x = \Delta y = 1$ μm, and propagation distance $Z = 600$ μm; (b) $\beta = 10°$, $\Delta x = \Delta y = 2$ μm, and $Z = 600$ μm; and (c) $\beta = 30°$, $\Delta x = \Delta y = 1$ μm, and $Z = 600$ μm.

4. APPLICATION IN COMPUTER-GENERATED HOLOGRAM (CGH) AND EXPERIMENTAL RESULTS

A. Simulation of Hologram Using Translated-ASM

The proposed Translated-ASM can be directly applied to signal processing in the titled-axis hologram reconstruction. To apply this technique to holographic applications, a spatial light modulator (SLM) is used to generate an interference pattern between the object and the reference field. The object field (E_o), propagated from the object plane, interferes with a conjugated reference beam (E_r^*) on the SLM plane, which is placed at a designated distance of Z_0 from the object plane (Fig. 6).

The interference intensity at the SLM plane is given by

$$I(x', y') = |E_r^* + E_o|^2 = |E_r^*|^2 + |E_o|^2 + 2\,\mathrm{Re}.[E_r^* E_o]. \tag{15}$$

Using our Translated-ASM in Eq. (13), the interference between E_o and E_r^* can be expressed as

$$E_r^* E_o(x', y') = |E_r|^2 \cdot \mathcal{F}^{-1}\{\mathcal{F}[m(x, y)] \exp[i(\vec{\kappa} - \vec{\mathbf{k}}_\mathbf{0}) \cdot \vec{\mathbf{r}}]\}. \tag{16}$$

Note that the product of the reference field and the conjugated field term is reduced to the intensity of the reference plane wave ($E_r E_r^* = |E_r|^2$). In the reconstruction of a hologram using a phase-type SLM, the phase information $\phi(x', y')$ can be extracted from the real part of the interference between E_o and E_r^* as in Eq. (17). In addition, the corresponding phase image, $P(x', y')$, generates a modulation pattern on the SLM plane of the reference field. Here, the intensity of the reference field (I_r) was normalized to 1 in Eqs. (17) and (18):

$$\phi(x', y') = \mathrm{Re}.(\mathcal{F}^{-1}\{\mathcal{F}[m(x, y)] \exp[i(\vec{\kappa} - \vec{\mathbf{k}}_\mathbf{0}) \cdot \vec{\mathbf{r}}]\}), \tag{17}$$

$$P(x', y') = \exp[i\phi(x', y')]. \tag{18}$$

At first, we numerically investigated the diffraction field from an SLM plane to a tilted output plane. The phase modulation images, encoded by the conventional on-axis ASM and the above Translated-ASM, were assumed to be placed on the SLM plane. The diffracted fields from the SLM plane were calculated by the Translated-ASM and compared in Fig. 7 for various propagation distances.

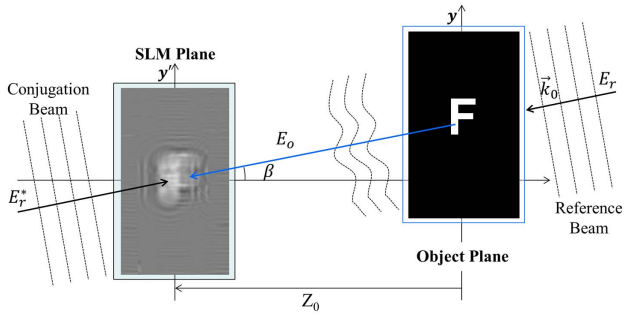

Fig. 6. Application to a holographic encoding on the SLM plane.

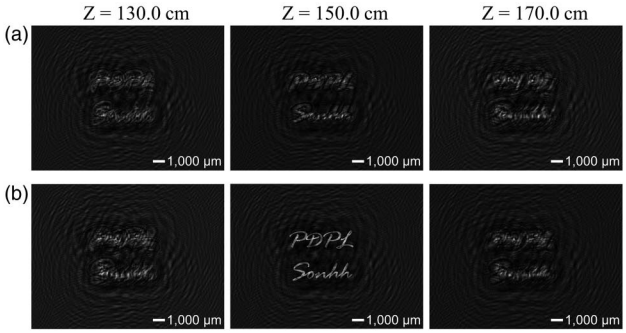

Fig. 7. Simulation results for the holographic images at various propagation distances using (a) on-axis ASM and (b) Translated-ASM.

Here, the sampling intervals are $\Delta x = \Delta y = 20$ μm, and the sampling numbers are $N_x = 800$, $N_y = 600$, which correspond to the physical parameters of the SLM used in the experiment. We assumed the designated distance of $Z_0 = 150$ cm and a tilt angle of $\beta = 15°$ in this simulation. The diffracted image calculated by our Translated-ASM showed a clear reconstruction image at the designated distance ($Z_0 = 150$ cm), as shown in Fig. 7(b). However, the on-axis ASM results did not provide images as clear as Translated-ASM over the whole distance range [Fig. 7(a)]. A better resolved image reconstruction was obtained using Translated-ASM, which clearly confirmed the validity of the proposed method on a tilted-axis holography.

B. Experimental Setup and Results

The holographic setup is further implemented. Figure 8 shows the geometrical configuration used in this experiment. An He–Ne laser at the wavelength of 632.8 nm was linearly polarized by a polarizer. The polarized light was collimated to form a plane wave by two lenses and illuminated to a reflective phase-type SLM (HAMAMATSU X10468) at a tilted angle of $\beta = 15°$ with respect to the horizontal direction.

The SLM had 800 × 600 pixels with the pixel pitch of 20 μm, and its effective area was 16.0 mm × 12.0 mm. The charge-coupled device (CCD) camera, which had a

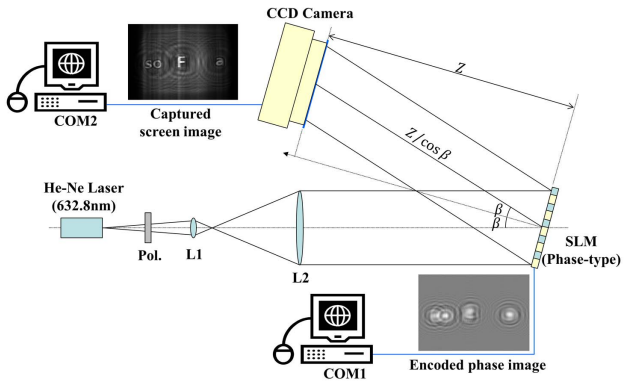

Fig. 8. Experimental arrangements of holographic reconstruction on a tilted axis. (Pol., polarizer; COM, computer; SLM, spatial light modulator.)

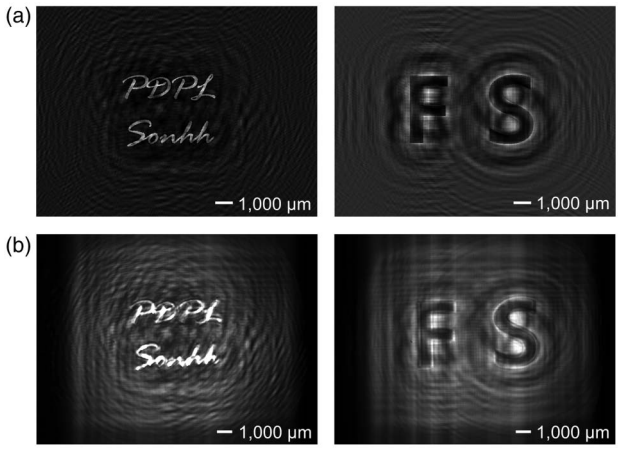

Fig. 9. Reconstructed images at $Z = 150$ cm: (a) Translated-ASM simulation images and (b) holography experimental images.

definition of 3296 × 2472 pixels and an effective area of 18.0 mm × 13.6 mm, was placed parallel to the surface of the SLM at a designated distance of $Z_0 = 150$ cm. The phase modulation image given by Eq. (18) was displayed on the SLM, and diffracted images were collected by the CCD camera.

The images generated by Translated-ASM are shown in Fig. 9(a) and the experimentally reconstructed images captured by the CCD camera are shown in Fig. 9(b). We observed almost the same intensity distributions in these images, including diffraction backgrounds.

We successfully confirmed that our Translated-ASM provided accurate and consistent holographic images, in the tilted-axis geometry with a large tilt angle, which validates our formulation once again.

5. CONCLUSION

A new method to accurately calculate diffraction fields between parallel planes along a tilted axis was proposed. The Translated-ASM was rigorously derived from a conventional angular spectrum method assuming the oblique plane wave incidence. Validity of the proposed Translated-ASM in a wide tilt angles and broad sampling intervals was confirmed by successfully simulating diffraction images without any false image shifts that have not been avoidable in prior methods. Translated-ASM formulation was further applied to reconstruction of holographic images on off-axis geometry with a large tilted angle, and it provided clear image formation which was not obtainable in prior methods. Using a phase-type spatial light modulator, we experimentally reconstructed holographic images, which showed good agreements with the simulation results of the Translated-Plane ASM. In both numerical simulation and experiments, we could confirm the validity of the proposed method, and it could find a high potential in design of wide-angle holograms and off-axis holographic microscopy.

REFERENCES

1. M. K. Kim, *Digital Holographic Microscopy* (Springer, 2011), Chap. 2.3.

2. J. W. Goodman, *Introduction to Fourier Optics*, 2nd ed. (McGraw-Hill, 1996), Chap. 2.2.
3. I. Yamaguchi, J. Kato, and J. Mizuno, "Image formation in phase-shifting digital holography and applications to microscopy," Appl. Opt. **40**, 6177–6186 (2001).
4. S. C. Lai, B. King, and M. A. Neifeld, "Wave front reconstruction by means of phase-shifting digital in-line holography," Opt. Commun. **173**, 155–160 (2000).
5. T. Shimobaba, N. Masuda, and T. Ito, "Simple and fast calculation algorithm for computer-generated hologram with wavefront recording plane," Opt. Lett. **34**, 3133–3135 (2009).
6. T. Kozacki, G. Finke, P. Garbat, W. Zaperty, and M. Kujawiska, "Wide angle holographic display system with spatiotemporal multiplexing," Opt. Express **20**, 27473–27481 (2012).
7. S. J. Jeong and C. K. Hong, "Pixel-size-maintained image reconstruction of digital holograms on arbitrarily tilted planes by the angular spectrum method," Appl. Opt. **47**, 3064–3071 (2008).
8. K. Matsushima, H. Schimmel, and F. Wyrowski, "Fast calculation method for optical diffraction on tilted planes by use of the angular spectrum of plane waves," J. Opt. Soc. Am. A **20**, 1755–1762 (2003).
9. N. Delen and B. Hooker, "Free-space beam propagation between arbitrarily oriented planes based on full diffraction theory: a fast Fourier transform approach," J. Opt. Soc. Am. A **15**, 857–867 (1998).
10. A. Dutt and V. Rokhlin, "Fast Fourier-transforms for nonequispaced data," Appl. Comput. Harmon. Anal. **2**, 85–100 (1995).
11. A. F. Ware, "Fast approximate Fourier transforms for irregularly spaced data," SIAM Rev. **40**, 838–856 (1998).
12. K. Matsushimal and T. Shimobaba, "Band-limited angular spectrum method for numerical simulation of free space propagation in far and near fields," Opt. Express **17**, 19662–19673 (2009).
13. R. P. Muffoletto, J. M. Tyler, and J. E. Tohline, "Shifted Fresnel diffraction for computational holography," Opt. Express **15**, 5631–5640 (2007).
14. K. Matushima, "Shifted angular spectrum method for off-axis numerical propagation," Opt. Express **18**, 18453–18463 (2010).
15. J. D. Jackson, *Classical Electrodynamics*, 3rd ed. (Wiley, 1998), Sect. 10.1.